Temperature and field dependent magnetization in a sub-μm patterned Co/FeRh film studied by resonant x-ray scattering

Lounès Lounis, Carlo Spezzani, Renaud Delaunay, Franck Fortuna, Martin Obstbaum, Stefan Günther, Christian H. Back, Horia Popescu, Franck Vidal, Maurizio Sacchi

Temperature and field dependent magnetization in a sub-µm patterned Co/FeRh film studied by resonant x-ray scattering

Lounès Lounis[1,2], Carlo Spezzani[3,4], Renaud Delaunay[5], Franck Fortuna[6], Martin Obstbaum[7], Stefan Günther[7], Christian H. Back[7], Horia Popescu[8], Franck Vidal[1], Maurizio Sacchi[1,8]

[1] *Sorbonne Universités, UPMC Univ Paris 06, CNRS UMR 7588, Institut des NanoSciences de Paris, 75005, Paris, France.*

[2] *Ecole Normale Supérieure, PSL Research University, 75231 Paris, France.*

[3] *ELETTRA – Sincrotrone Trieste, Area Science Park, 34149 Trieste, Italy.*

[4] *Université Paris-Sud, CNRS-UMR 8502, Laboratoire de Physique des Solides, Bât. 510, 91405 Orsay, France.*

[5] *Sorbonne Universités, UPMC Univ Paris 06, CNRS UMR 7614, Laboratoire de Chimie Physique Matière et Rayonnement, 75005 Paris, France.*

[6] *Université Paris-Sud, CNRS UMR 8609, Centre de Sciences Nucléaires et de Sciences de la Matière, Bât. 104-108, 91405 Orsay, France.*

[7] *Fakultät für Physik, University of Regensburg, 93053 Regensburg, Germany.*

[8] *Synchrotron SOLEIL, L'Orme des Merisiers, Saint-Aubin, B.P. 48, 91192 Gif-sur-Yvette, France.*

Abstract

We studied the temperature and field dependence of the magnetization in a Co/FeRh/MgO(001) film patterned into a matrix of sub-µm sized rectangles, using element selective resonant scattering of polarized soft x-rays. We show that it is possible to reverse partially the magnetization of the Co layer in a thermal cycle that crosses the FeRh antiferromagnetic to ferromagnetic transition. Our results support the interest of patterned Co/FeRh films and their potential for achieving temperature induced magnetization switching.

1. Introduction

Developing thermally induced magnetization switching (TIMS), where the temperature control of intrinsic material properties drives a deterministic reversal of the local magnetization, has considerable applicative interest. The combination of materials with different temperature dependent magnetic properties has been used, for instance, to switch the magnetization with a single laser pulse in rare-earth–transition-metal ferrimagnetic

compounds, in a process that combines thermal and photon helicity dependent effects [1]. Controlling the local temperature by a laser pulse is also at the basis of heat assisted magnetic recording processes that were proposed to significantly lower the external field values necessary for switching a magnetic bit [2]. A different approach to TIMS makes use of substrates whose intrinsic magnetic properties feature regular spatial modulations generating local surface dipolar fields that can be controlled by tuning the temperature [3]. The proof-of-principle of this approach made use of a thin ferromagnetic (FM) Fe layer deposited on a magnetically active MnAs/GaAs(001) template [4, 5]. It was shown that it is possible to control the Fe magnetization in Fe/MnAs/GaAs(001) by finely tuning the temperature at ambient. Element selective x-ray resonant magnetic scattering (XRMS) experiments demonstrated that various magnetic configurations of the Fe/MnAs system are stabilized predictably by acting on the thermal cycle parameters and on the presence of a bias field [5]. What one actually does by changing the temperature is to control the surface dipolar fields associated with the template magnetic microstructure, and, ultimately, vary the effective magnetic field acting on the overlayer. Time-resolved experiments showed the potential of this approach for fast magnetization switching, where local temperature changes are triggered by a single optical laser pulse [6].

MnAs/GaAs(001), featuring temperature controlled self-organized ferro/para-magnetic stripes [7], is a useful test case for achieving TIMS by using a magnetically active template, but it is not a practical material for applications. Apart from requiring a complex preparation by molecular beam epitaxy (MBE), the paramagnetic to FM transition in MnAs takes place for decreasing temperatures (while the opposite would be preferable) and at values that are too close to ambient (20-40°C) for ensuring the thermal stability of a real device. In the search for alternatives to Fe/MnAs, we have identified patterned Co/FeRh films as promising candidates for designing more advantageous TIMS systems that work on the principle of a magnetically active template.

The equiatomic α'-phase of cubic FeRh undergoes a first-order magnetic phase transition at ~100 °C from low-T antiferromagnetic (AF) to high-T FM order, accompanied by a 1% volume expansion of the unit cell [8]. The temperature dependent magnetization curve shows a hysteresis over a thermal cycle, as expected for a first order phase transition. The width of the hysteresis and other details of the magnetostructural transition are sensitive to the composition [9], to the strain [10] and, in thin films, to the thickness [11], and can be controlled by applying electric [12] or magnetic [13] fields. High crystalline quality FeRh

films can be grown by magnetron sputtering, notably on MgO(001) crystalline substrates [2, 11, 13].

The basic features that characterize the system that we have devised are:

- a template (FeRh) that features no net magnetization at ambient (AF state), and becomes FM at higher temperature [2, 8-14];
- a regular lateral confinement (sub-micrometer dots) that, in the FeRh FM phase, generates a dipolar field H_D extending above the surface of the dot;
- an external bias field H_{ext} ($< H_D$) that aligns the FeRh dot during its transition to the FM state;
- a FM overlayer (Co) with coercive field H_C such that $H_{ext} < H_C < H_D$.

When these conditions are met, the Co magnetization direction will be oriented according to the sign of H_{ext} by performing a thermal cycle that encompasses the FeRh magnetic transition. This scheme is particularly interesting in view of controlling the local temperature by a focused laser pulse that induces the FeRh phase transition, modifies the surface dipolar field and reverses the Co magnetization only over the irradiated area (ideally, over a single dot). At the end of the thermal cycle, the Co magnetic configuration will depend on the bias field strength and orientation. The process is similar to thermally assisted magnetization reversal in FePt/FeRh [2, 15], yet with the template-generated dipolar field contributing to the effective magnetic field acting on the Co layer [5, 16].

Here we report on the study of the Co and Fe magnetic response in Co/FeRh/MgO(001) patterned films by using element selective resonant magnetic scattering of polarized soft X rays. Previous XRMS work on Fe/MnAs [4-6] demonstrated that element selectivity is a useful complement to other magnetometry techniques for a detailed analysis of field and temperature dependent magnetization curves that are tangled and complex.

2. Experimental details

A 50 nm thick FeRh film with (001) orientation was grown by magnetron sputtering from a single equiatomic target onto a MgO(001) substrate at the Center for Magnetic Recording Research of the University of California, San Diego [17]. Using a mask, a 5 nm Co layer was deposited on half of the FeRh film. Finally, a 2 nm Au layer was deposited on the whole sample for protecting the surface against contamination. The sample was patterned into two 0.5×0.5 mm^2 areas using optical lithography and ion etching, according to the sketch of Fig. 1. The area on the FeRh side was left intact and served as a reference of the continuous FeRh

film without Co and after etching. The area on the Co/FeRh side was patterned into a matrix of 400×800 nm^2 rectangles.

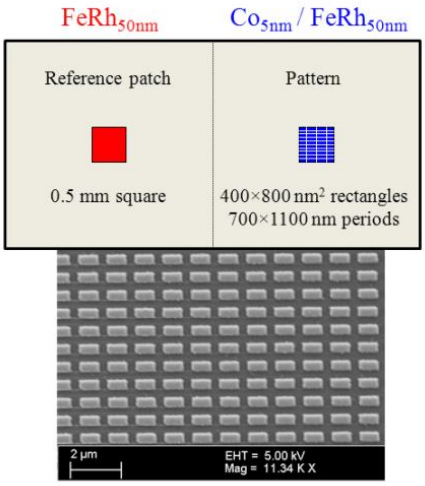

Figure 1. Top: sketch of the sample lithographic preparation, showing the FeRh reference patch and the pattern of 400×800 nm^2 rectangles etched in the Co/FeRh film. Bottom: scanning electron microscopy image of the pattern (the white scalebar is 2 µm).

Resonant scattering measurements were performed at the Circular Polarization beamline of the Elettra synchrotron (Trieste, Italy), using the IRMA reflectometer [18]. The sample was mounted on a holder that comprised an electromagnet, capable of applying a field of up to 1.7 kOe along any in-plane direction, and a thermoelectric cooler covering the temperature range from -10 to +140 °C. Slitted photodiodes with varying angular acceptance were installed on the detector arm. Soft X rays of selectable polarization (either linear, vertical and horizontal, or circular with positive and negative helicity) delivered by an electromagnetic undulator were tuned in energy to the Fe-2p and Co-2p resonances (700–800eV range) using a grating monochromator. Specular reflectivity provides spatially averaged but element resolved magnetization curves as a function of the sample temperature T and of the bias field H_{ext} [5]. For the patterned sample, one can monitor the magnetic signal originating from regular repeats over the ensemble of the objects by measuring at sample angle positions that correspond to Bragg peaks in the rocking scan [19].

3. Results and discussion

First we measured specular reflectivity from the reference FeRh patch, in order to check for the reliability of the sample properties after the lithography procedure. Data were collected as

a function of photon energy and scattering angle for determining the conditions that optimize the magnetic signal.

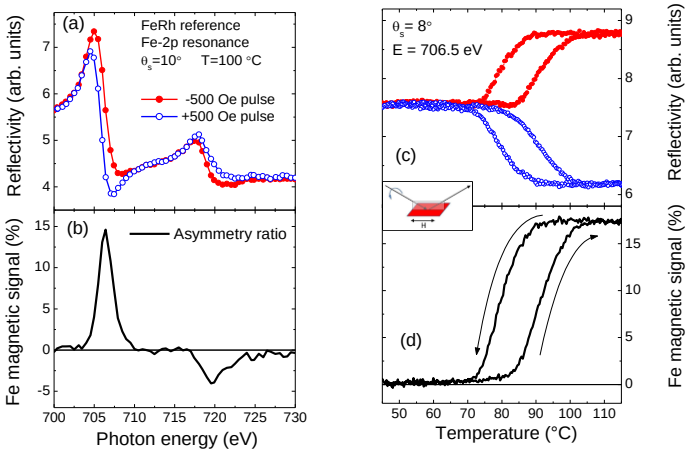

Figure 2. Specular reflectivity from the FeRh reference sample. Each point is measured at remanence after applying a 500 Oe magnetic pulse of negative (●) or positive (○) sign. (a) Photon energy dependence across the Fe-2p resonance, at θ_S = 10° and T = 100 °C, and (b) corresponding magnetic signal (▬) defined as the difference between data obtained for opposite signs of the magnetic pulse divided by their sum. (c) Temperature dependent reflectivity at 706.5 eV and θ_S = 8°, and (d) corresponding magnetic signal showing the AF→FM→AF transition over the thermal cycle. The inset sketches the experimental geometry.

The photon energy and temperature dependence of the magnetic signal at the Fe-2p resonance is shown in Fig. 2. The magnetic signal is defined as an asymmetry ratio, i.e. as the difference between data obtained at remanence after magnetic pulses of opposite sign divided by their sum. Measurements over a thermal cycle that spans the 40-115 °C range show that FM saturation is attained at ~105°C upon heating and that the system returns to its AF state at ~70 °C when cooling down, with a ~12 °C width at mid-height of the hysteresis loop. These values are characteristic of a good quality FeRh thin film. With the photon energy tuned to the Fe-2p core resonance, the dependence of the specular reflectivity on the applied magnetic field can be used to draw element selective hysteresis loops as shown in Fig. 3, which compares two curves obtained at a sample temperature of 91 and of 113 °C.

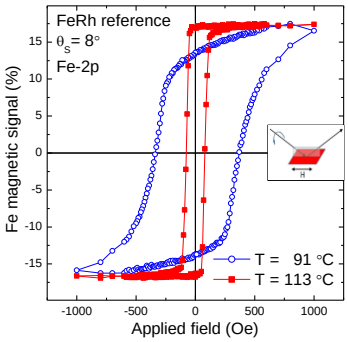

Figure 3. Field dependent specular reflectivity at the Fe-2p resonance from the FeRh reference patch at T = 91 (○) and 113 (■) °C. The magnetic signal in the hysteresis loop is defined as the measured reflectivity minus its average over a complete cycle, divided by the average.

The element selectivity of resonant magnetic scattering becomes important when moving to the Co/FeRh pattern (Fig. 4). The 2p resonances of Fe and Co are well separated, making it easy to identify individual contributions from the two elements in the temperature and field dependent magnetic signal, by simply tuning the photon energy to the appropriate range. The sign of the magnetic signal in a resonant scattering experiment depends on several parameters beyond the magnetization orientation [20], notably the sample vertical structure and the scattering angle: this explains why the sign of the Fe magnetic signal changes between Fig. 2b and 4b.

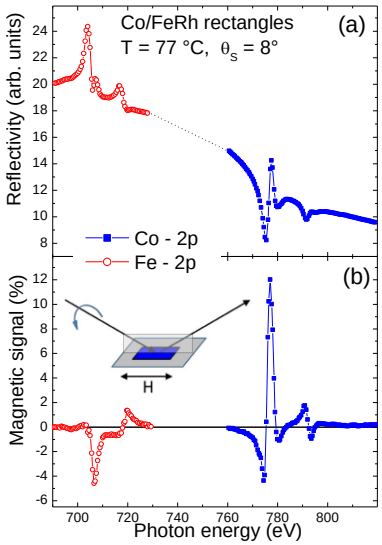

Figure 4. Photon energy dependent specular reflectivity (a) and magnetic signal (b) from the Co/FeRh pattern of rectangles. T = 77 °C, θ_S=8°. The photon energy range covers the 2p resonances of Fe (○) and Co (■).

When measuring the patterned area, one can collect, in addition to the specular reflectivity, the diffracted signal from the regular repeat of the dots by performing a rocking scan, i.e. by scanning the sample angle θ_S at fixed detector angle θ_D [19]. In co-planar geometry, this corresponds to varying the component q_x of the scattering vector **q** that projects along the intersection between the *xy* sample surface and the *xz* vertical scattering plane. Defining $\Delta\theta$ as the off-specular angle (θ_S - $\theta_D/2$), one has $q_x = (4\pi/\lambda)\cdot\sin(\theta_D/2)\cdot\sin(\Delta\theta)$, λ being the photon wavelength. Peaks in the scattered intensity are observed when $2\pi n/q_x$ (*n* integer) matches the period *d* of the array [21].

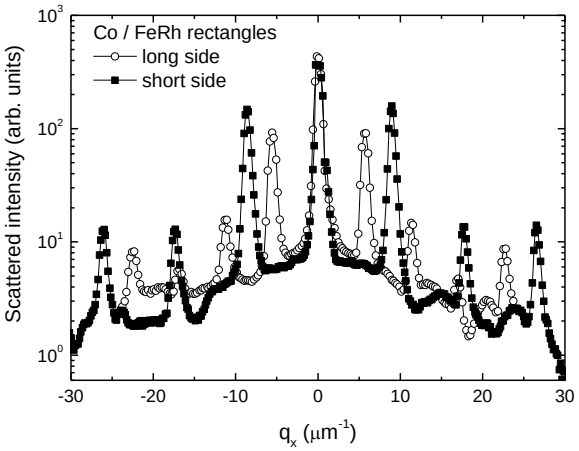

Figure 5. Scattered intensity *vs.* sample angle at fixed detector angle (rocking scan). The intensity is plotted against the in-plane exchanged momentum $q_x=(4\pi/\lambda)[\sin(\theta_D/2)\cdot\sin(\Delta\theta)]$, where $\Delta\theta$ is the off-specular angle. Bragg peaks of n^{th} order identify the period $d=2\pi n/q_x$ of the pattern of rectangles along their minor (d=720 nm) and major (d=1120 nm) sides.

Fig. 5 shows the result of two rocking scans measured for the Co/FeRh pattern, with either the short (■) or the long (○) side of the rectangles oriented along the *x* direction. The resulting periods, 720 nm and 1120 nm, match well the nominal values. Element specific magnetic signals can be measured as a variation of either the diffracted intensity or of the specular reflectivity, the former guaranteeing that the signal comes from the patterned area only [19].

Fig. 6 shows the magnetic signal in the specular reflectivity at the Co resonance, measured as a function of temperature (a) and of the applied field (b), along the short side of the rectangles. The thermal cycle data are collected in an applied field of 200 Oe, after a 1 kOe pulse. They show that when the temperature increases to ~75 °C and the FeRh initiates the transition to the FM phase, the Co magnetic signal steadily decreases and inverts its sign at

~85 °C, then remains constant and negative until the highest temperature is reached. In the cooling branch of the cycle, the Co signal crosses zero again at ~70 °C, and progressively recovers its initial value at ~50 °C. Although this is not the behavior that was sought for, since one does not reverse the Co magnetization at the end of the cycle, the changes with temperature of the magnetization sign (Fig. 6a) and of the shape of the hysteresis loops (Fig. 6b) are suggestive of the mechanism that we had devised, i.e. of the presence of dipolar fields at the surface of the dots in the FeRh FM phase.

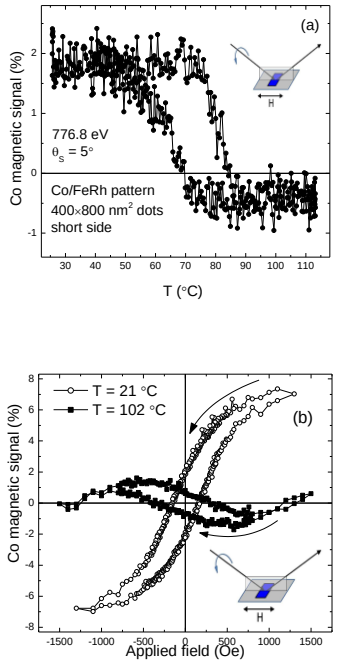

Figure 6. Co magnetization in the patterned Co/FeRh film, probed along the short side of the rectangles. (a) Thermal cycle from RT up to 113 °C. Data are collected at H_{ext} = 200 Oe, after an initial 1 kOe pulse. (b) Hysteresis loops at 21 and 102 °C, showing opposite sign of the Co remanent magnetization.

A similar behavior is observed when applying the field parallel to the long side of the rectangles. Fig. 7 compares the result of a thermal cycle in a 200 Oe bias field at the Co and at the Fe resonant photon energies. Data are collected in diffraction conditions, after a 1.5 kOe magnetic pulse. The main difference with Fig. 6a is that the Co magnetization, after having changed sign at a slightly higher temperature, vanishes at ~110 °C. On the cooling branch, it recovers its initial value at ~50 °C, as it was the case in Fig. 6a.

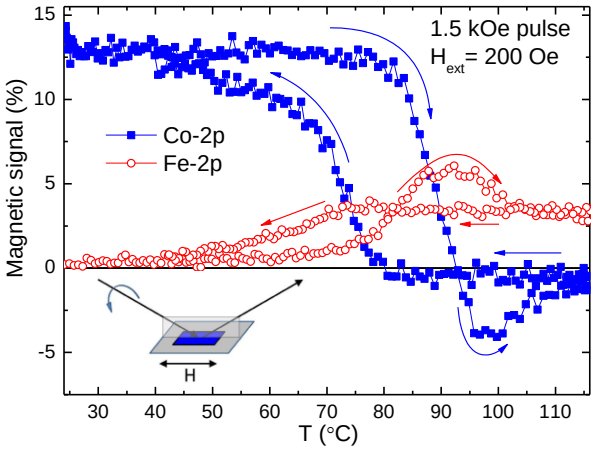

Figure 7. Fe (○) and Co (■) magnetic signal in the diffracted intensity from the pattern of rectangles in a thermal cycle from RT up to 115 °C. The magnetization is probed parallel to the long side of the rectangles. After an initial 1500 Oe pulse, data are collected *vs.* temperature in a field H_{ext} = 200 Oe.

In order to understand better the Co magnetization behavior in the thermal cycle, we plot again in Fig. 8 the same Co data reported in Fig. 7, together with Co-specific hysteresis loops measured at seven different temperatures along the heating branch of the cycle. Up to 75 °C, there is no significant change in the shape of the loops. A reduction of the coercive field from ~300 to ~220 Oe is evidenced at 82 °C. Starting from ~90 °C, the curves display two shifted loops centered at ~1 kOe and a reversed sign of the remanent Co magnetization.

Shrinking of the hysteresis loop begins at the same temperature that corresponds to the FeRh turning ferromagnetic. A similar effect, albeit with different coupling configurations, has been observed previously in other FM/FeRh bilayers [2, 22] and was attributed to exchange coupling at the FM/FeRh interface. The behavior observed at temperatures above 90 °C, though, cannot be associated to direct exchange only. We interpret these curves as due to the combined action of the external field and of the surface dipolar field generated by the ferromagnetic dots, the same mechanism at the basis of the temperature driven Fe magnetization reversal observed in Fe/MnAs (see, e.g., Fig. 2b of ref. [5]).

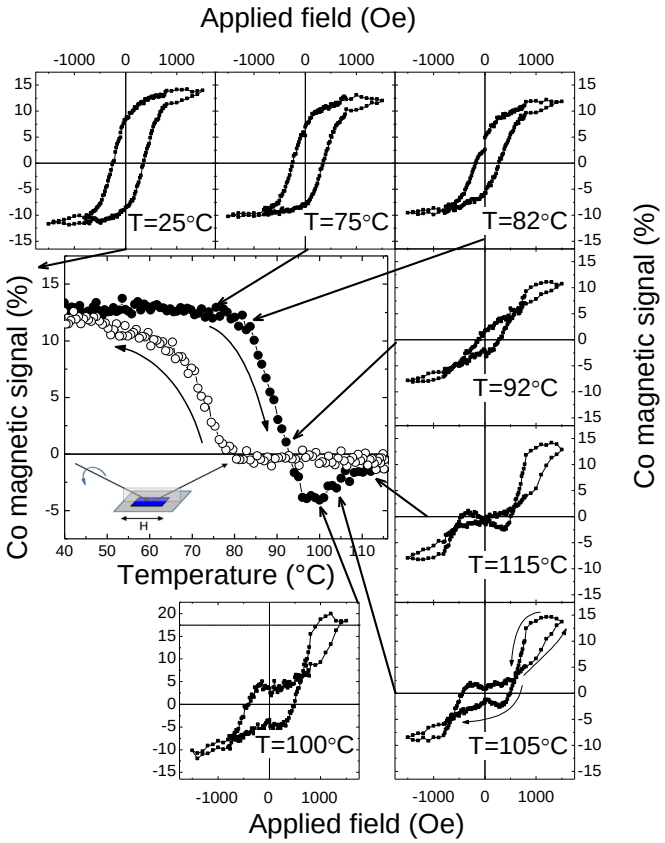

Figure 8. Co magnetic signal in the patterned Co/FeRh film, probed parallel to the long side of the rectangles. The central panel shows the same Co data of Fig. 7, i.e. a thermal cycle from RT up to 115 °C (●) and back (○). Hysteresis loops measured at seven different temperatures along the heating branch of the thermal cycle are also shown. Note the reversed sign of the remanent Co magnetization above ~90 °C (see arrows in the T = 105 °C panel), as well as the high temperature side loops centered at ~1 kOe.

The intensity of the dipolar field H_D acting on Co at the surface of the FeRh dot is proportional to the FeRh magnetization M^{FeRh}, which itself depends on H_{ext} and on T, i.e. $H_D = - \alpha M^{FeRh} (H_{ext}, T)$. Therefore, the Co magnetization in the external field H_{ext} is determined by the effective field $H_{ext}+H_D$ and depends on the FeRh magnetization [5].

Fig. 9 illustrates schematically how the strength of H_D can modify the shape of the Co hysteresis loop as a function of H_{ext}. The $H_D=0$ curve in Fig. 9 is chosen arbitrarily to mimic the Co hysteresis curve at low temperature, when the FeRh magnetization can be neglected. For increasing values of H_D, the shape of the Co magnetization dependence on H_{ext} varies producing, in particular, a sign change at remanence [5]. Comparing the curves in Fig. 9 with the experimental Co hysteresis data in Fig. 8 provides a rough estimate of H_D: in the FeRh FM phase dipolar fields of the order of 500-600 Oe are present at the surface of the dots and

parallel to their long side. Higher values in excess of 1 kOe are estimated along the rectangles short side (Fig. 6b).

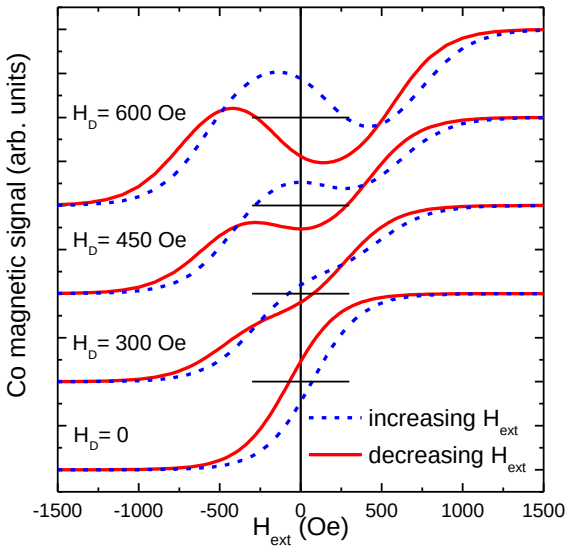

Figure 9. Co hysteresis curves in presence of a dipolar field H_D proportional to the FeRh magnetization (dashed and full lines are for increasing and decreasing H_{ext} values, respectively). At $H_D = 0$ (bottom), the curves are arbitrarily set to mimic the room temperature Co hysteresis loop. The other curves are calculated by adding a dipolar field H_D proportional to the FeRh T-dependent magnetization. Bottom to top, they correspond to a maximum dipolar field of 300, 450 and 600 Oe.

4. Conclusion

We have prepared and measured an array of Co/FeRh sub-µm rectangular dots, probing the Co and Fe magnetic properties selectively by X-ray resonant magnetic scattering. We point out properties and behaviors of the Co overlayer magnetization that we correlate with the lateral confinement of the FeRh template and that are relevant for thermally induced magnetization switching processes. The element selective thermal cycles and hysteresis loops provide a first indication of the temperature induced Co magnetization switching, driven by the FeRh dots becoming ferromagnetic. We estimate that local dipolar fields of up to 500–1000 Oe can be turned on by acting on the temperature. The interest of FeRh is twofold: i) it can be prepared by sputtering, a process that is easier to implement than MBE; ii) it is AF at ambient, and it turns FM at temperatures that are high enough to guarantee room temperature stability and low enough to be accessible by laser pulse heating [17, 23-25]. Further work is needed for assessing and optimizing the many parameters (e.g., thickness of the FeRh and Co layers, dot shape and size) intervening in the definition of the structure of these objects and in the experimental conditions for achieving TIMS. In particular, introducing a non-magnetic

spacer layer may help decoupling the Co and FeRh films limiting a direct interlayer exchange, which can hamper the temperature driven Co magnetization reversal. Care must be exerted, though, since it is known that overlayers can alter the properties of FeRh films close to their surface [26].

Although we have not achieved yet the objective of a stable temperature driven switching of the FM overlayer at ambient, our study shows that patterned FeRh has potential for becoming a viable alternative to MnAs as a template for generating temperature controlled local dipolar fields.

Acknowledgements

Our thanks go to Vojtěch Uhlíř and Eric E. Fullerton, Center for Magnetic Recording Research, University of California San Diego, for providing the FeRh/MgO film. We gratefully acknowledge the help and advice from Vincent Garcia and Stéphane Fusil (Unité Mixte de Physique CNRS/Thales, Orsay). We would like to extend our thanks to Sincrotrone Trieste for granting our project beam time and to the Circular Polarization beamline staff for assistance during the experiment. This work was supported in part by the RTRA Triangle de la physique, under Grant No. 2009-082T FibNanoSynth, and by CNRS, within the 2014 PEPS_SASLELX program.

References

1. Kimel A V, Kirilyuk A, Tsvetkov A, Pisarev R V and Rasing T 2004 *Nature* **429**, 850; Kirilyuk A, Kimel A V and Rasing T 2013 *Rep. Prog. Phys.* **76**, 026501; Hassdenteufel A, Hebler B, Schubert C, Liebig A, Teich M, Helm M, Aeschlimann M, Albrecht M and Bratschitsch R. 2013 *Adv. Mater.* **25**, 3122; Mangin S *et al.* 2014 *Nature Mater.* **13**, 286.
2. Thiele J-U, Maat S and Fullerton E E 2003 *Appl. Phys. Lett.* **82**, 2859; Thiele J-U, Maat S, Robertson J L and Fullerton E E 2004 *IEEE Trans. Mag.* **40**, 2537.
3. Marangolo M and Sacchi M. *Method for changing the direction of magnetization in a ferromagnetic layer*. 2011 French patent n. 2947375.
4. Sacchi M, Marangolo M, Spezzani C, Breitwieser R, Popescu H, Raches Salles B, Delaunay R, Eddrief M and Etgens V 2010 *Phys. Rev. B* **81**, 240801(R).
5. Spezzani C, Vidal F, Delaunay R, Eddrief M, Marangolo M, Etgens V, Popescu H and Sacchi M 2015 *Sci. Rep.* **5**, 8120.
6. Spezzani C *et al.* 2014 *Phys. Rev. Lett.* **113**, 247202.
7. Däweritz L. 2006 *Rep. Prog. Phys.* **69**, 2581.

8. Kouvel J S and Hartelius C C 1962 *J. Appl. Phys.* **33** 1343.
9. Van Driel J, Coehoorn R, Strijkers G J, Brück E and de Boer F R 1999 *J. Appl. Phys.* **85** 1026.
10. Ohtani Yand Hatakeyama I 1994 *J. Magn. Magn.Mater.* **131**, 339.
11. Suzuki I, Koike T, Itoh M, Taniyama T and Sato T 2009 *J. Appl. Phys.* **105**, 07C717.
12. Cherifi R O *et al*. 2014 *Nature Materials* **13**, 345.
13. Maat S, Thiele J U and Fullerton E E 2005 *Phys. Rev. B* **72**, 214432.
14. Stamm C *et al.* 2008 *Phys. Rev. B* **77**, 184401.
15. Naito T *et al*. 2011 *J. Appl. Phys.* **109**, 07C911.
16. Breitwieser R, Marangolo M, Lüning J, Jaouen N, Joly L, Eddrief M, Etgens V and Sacchi M 2008 *Appl. Phys. Lett.* **93**, 122508.
17. Günther S *et al.* 2014 *Phys. Rev. B* **90**, 180407(R).
18. Sacchi M, Spezzani C, Torelli P, Avila A, Delaunay R and Hague C F 2003 *Rev. Sci. Instrum.* **74**, 2791.
19. Spezzani C, Fabrizioli M, Candeloro P, DiFabrizio E, Panaccione G and Sacchi M 2004 *Phys. Rev. B* **69** 224412.
20. Sacchi M, Mirone A, Hague C F, Mariot J-M, Pasquali L, Isberg P, Gullikson E M, Underwood J H 1999 *Phys. Rev. B* **60**, R12569; Sacchi M, Mirone A, Hague C F, Castrucci P, Gunnella R, DeCrescenzi M 2001 *Phys. Rev. B* **63**, 012403.
21. Daillant J and Gibaud A 1999 X-ray and neutron reflectivity: principles and applications Berlin, Springer; Jergel M *et al*. 1999 *J. Phys. D Appl. Phys.* **32**, A220; Ulyanenkov A *et al*. 2001 *J. Phys. D Appl. Phys.* **34**, A179.
22. Zhou T J, Cher K, Hu J F, Yuan Z M and Liu B 2012 *J. Appl. Phys.* **111**, 07C116; I. Suzuki, Y. Hamasaki, M. Itoh, and T. Taniyama, Appl. Phys. Lett. **105**, 172401 (2014).
23. Ju G, Hohlfeld J, Bergman B, van deVeerdonk R J M, Mryasov O N, Kim J Y, Wu X, Weller D and Koopmans B 2004 *Phys. Rev. Lett.* **93**, 197403.
24. Thiele J U, Buess M and Back C H 2004 *Appl. Phys. Lett.* **85**, 2857; Radu I, Stamm C, Pontius N, Kachel T, Ramm P, Thiele J U, Dürr H A and Back C H 2010 *Phys. Rev. B* **81**, 104415; Mariager S O *et al.* 2012 *Phys. Rev. Lett.* **108**, 087201.
25. Quirin F *et al.* 2012 *Phys. Rev. B* **85**, 020103(R).
26. Fan R *et al.* 2010 *Phys. Rev. B* **82**, 184418; Baldasseroni C *et al.* 2014 *J. Appl. Phys.* **115**, 043919.